Metal−Organic Framework Nodes as Nearly Ideal Supports for Molecular Catalysts: NU-1000- and UiO-66-Supported Iridium Complexes

Dong Yang,[†] Samuel O. Odoh,[‡] Timothy C. Wang,[§] Omar K. Farha,[§,∥] Joseph T. Hupp,[§] Christopher J. Cramer,[‡] Laura Gagliardi,*[,‡] and Bruce C. Gates*[,†]

[†]Department of Chemical Engineering & Materials Science, University of California, Davis, California 95616, United States
[‡]Department of Chemistry, Chemical Theory Center, and Supercomputing Institute, University of Minnesota, Minneapolis, Minnesota 55455-0431, United States
[§]Department of Chemistry, Northwestern University, 2145 Sheridan Road, Evanston, Illinois 60208, United States
[∥]Department of Chemistry, Faculty of Science, King Abdulaziz University, Jeddah 22254, Saudi Arabia

(S) *Supporting Information*

ABSTRACT: Metal−organic frameworks with Zr_6 nodes, UiO-66 and NU-1000, were investigated as supports for $Ir(CO)_2$ and $Ir(C_2H_4)_2$ complexes. A single bonding site for the iridium is identified on the nodes of NU-1000, whereas two sites are identified on UiO-66, although at low iridium loadings only one site is occupied. Density functional theory calculations provide structural results that are in good agreement with infrared and X-ray absorption fine-structure spectra. The reactivity of node-supported $Ir(CO)_2$ with C_2H_4 and the catalytic activity and selectivity of the species initially present as $Ir(C_2H_4)_2$ for ethylene hydrogenation and dimerization were investigated both experimentally and computationally and shown to be strongly influenced by the node.
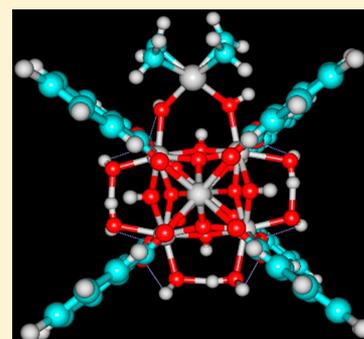
1. INTRODUCTION

Metal−organic frameworks (MOFs) are a class of crystalline and porous materials formed by coordination bonds between metal-containing nodes and organic linkers.[1−3] MOFs that are stable at high temperatures are appealing but still little-investigated as catalyst supports,[4−10] especially for transformations of gas-phase reactants. Several investigators have used the organic linkers of MOFs to anchor metal complexes used as catalysts. For example, Manna et al.[11] prepared MOFs with Fe(II) and Co(II) salicylaldimine complexes as linkers, finding them to be highly active for 1-octene hydrogenation. Fei and Cohen[12] modified the linkers of MOFs to form thiocatechol-functionalized sites for palladium centers that selectively catalyze the oxidative functionalization of aromatic C−H bonds. Gonzalez et al.[13] used an MOF with bipyridine sites in the linkers that reacted with $Ir(COD)_2BF_4$ (COD is 1,5-cyclooctadiene) to give a catalyst for arene C−H borylation. These catalysts are all comparable to organic polymer-supported catalysts.

Alternatively, MOF nodes that resemble small pieces of metal oxides have been used as catalyst supports that are comparable to metal oxides and zeolites. Larabi and Quadrelli[14] pointed out that the OH groups on such nodes provide sites for binding of organometallic catalyst precursors. For example, Nguyen et al.[15] used defect sites in the zirconium oxide nodes of UiO-66 as a support for a catalyst synthesized from vanadyl acetylacetonate to convert cyclohexene to benzene by oxidative dehydrogenation; this catalyst was used at temperatures up to 350 °C, pointing to stability advantages of this class of MOF. Mondloch et al.[16] also reported the use of such MOF nodes as supports for aluminum and zinc catalysts made by atomic layer deposition of gas-phase catalyst precursors.

Supported metal catalysts that are essentially molecular and structurally well-defined offer numerous advantages for fundamental understanding; such catalysts have been synthesized on the surfaces of zeolites and in prospect can be synthesized similarly on MOF nodes.[17] We now report such catalysts: MOF node-supported metal complexes that are structurally well-defined, from the viewpoints of both the metal species and the support. We selected Zr_6-based UiO-66 and NU-1000 frameworks because of their exceptional thermal stability and well-defined structures.[16,18] UiO-66 is composed of $[Zr_6(\mu_3\text{-}O)_4(\mu_3\text{-}OH)_4]^{12+}$ nodes, each linked to 12 carboxylates of terephthalate ligands to form tetrahedral and octahedral cages; however, there are many defects from missing linkers in this MOF, with the resulting otherwise open metal sites occupied by hydroxo ligands.[18−20] The node topology of NU-1000 has been determined to be $[Zr_6(\mu_3\text{-}O)_4(\mu_3\text{-}OH)_4(OH)_4(OH_2)_4]^{8+}$,[21] and it is coordinated to eight
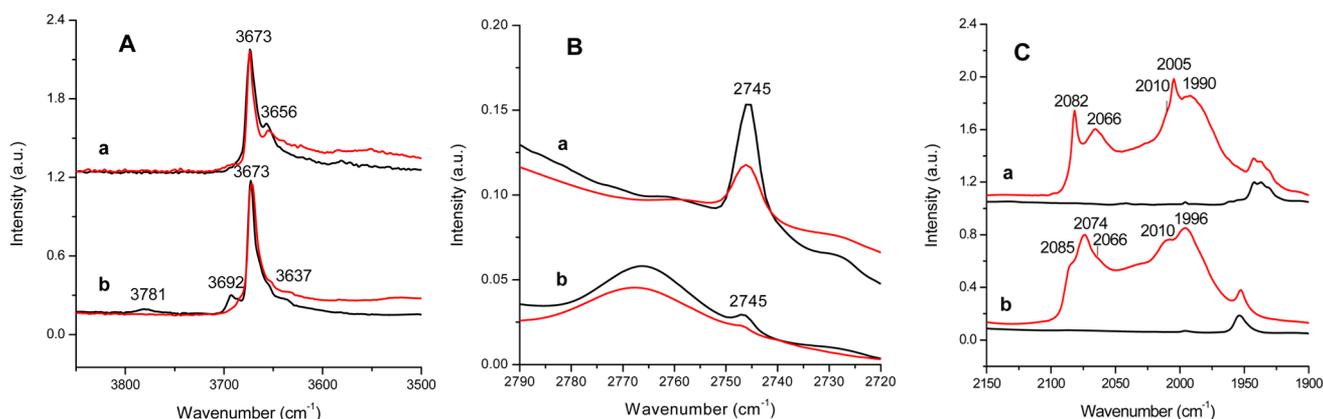
Figure 1. IR spectra in (A) v_{OH} region, (B) H-bonded H_2O and −OH region and (C) v_{CO} region characterizing bare NU-1000, a, and bare UiO-66, b, (black traces) and the samples formed by adsorption of $Ir(CO)_2(acac)$ on them (red traces).

tetratopic linkers of 1,3,6,8-tetrakis(p-benzoic-acid)pyrene (H_4TBAPy) to form triangular and hexagonal pores. We used $Ir(CO)_2(acac)$ (acac = acetylacetonate) and $Ir(C_2H_4)_2(acac)$ as precursors to react with functional groups such as OH on the nodes of NU-1000 and UiO-66, accompanied by removal of the acac ligands.[17] The samples were characterized by infrared (IR) and extended X-ray absorption fine-structure (EXAFS) spectroscopies as well as density functional theory (DFT) calculations. Our results demonstrate the presence of bonding between the Ir species and node sites and determine their catalytic properties for conversion of ethylene in the presence of H_2.

2. EXPERIMENTAL SECTION

2.1. Synthesis of UiO-66. $ZrCl_4$ (0.080 g, 0.343 mmol) and 0.7 mL of acetic acid (modulator) were dissolved in 20 mL of DMF in a 100 mL Teflon-capped glass jar by using ultrasound for 5 min. The linker precursor benzene-1,4-dicarboxylic acid (0.057 g, 0.343 mmol) was then added into the solution and dissolved by ultrasound applied for about 5 min. The jars were kept in an oven at 393 K under static conditions for 24 h. White precipitates were produced, and they were isolated by centrifugation after cooling to room temperature. The solids were washed with DMF three times to remove unreacted precursors and with methanol six times to remove DMF. Then, the powder was dried at room temperature.

2.2. Synthesis of NU-1000. A sample consisting of 97 mg of $ZrOCl_2 \cdot 8H_2O$ (0.30 mmol) and 2700 mg (22 mmol) of benzoic acid was mixed in 8 mL of DMF (in a 6 dram vial) and ultrasonically dissolved. The clear solution was incubated in an oven at 353 K for 1 h. After cooling to room temperature, 40 mg (0.06 mmol) of H_4TBAPy was added to this solution, and the mixture was sonicated for 20 min. The yellow suspension was held in an oven at 353 K for 24 h. After cooling to room temperature, yellow polycrystalline material was isolated by filtration (35 mg of activated material, 54% yield) and washed with DMF and subsequently activated with HCl. Then, the solid was washed twice with DMF and six times with acetone. The powder was dried at room temperature.

2.3. Synthesis of $Ir(CO)_2$ and $Ir(C_2H_4)_2$ Supported on MOFs. Sample syntheses and handling were performed with the exclusion of moisture and air by use of a double-mainfold Schlenk vacuum line and an argon-atmosphere glovebox.

The precursor $Ir(CO)_2(acac)$, with 98% purity, was purchased from Strem Chemicals, Inc. The precursor $Ir(C_2H_4)_2(acac)$ was synthesized as described elsewhere;[22] it has been characterized by X-ray diffraction crystallography and ^1H and ^{13}C NMR, Raman, and IR spectroscopies.

The supported iridium complex was prepared by bringing the precursor $Ir(CO)_2(acac)$ or $Ir(C_2H_4)_2(acac)$ (36.2 mg for a 10 wt % iridium loading or 3.6 mg for a 1.0 wt % iridium loading) in contact with 200 mg of activated MOF powder (UiO-66 or NU-1000 was

activated under vacuum (10^{-7} Torr) at 423 or 393 K, respectively, for 24 h before use) in a Schlenk flask and slurried in 40 mL of dried n-pentane (Fisher, 99%) at room temperature. After 4 h, the solvent was removed by evacuation for a day so that all the iridium remained in the MOF. The resultant solids, containing 10 or 1.0 wt % iridium, were stored in the argon-filled glovebox. The iridium loadings were inferred from the conditions of the syntheses, whereby all of the added iridium remained in the MOF.

2.4. Infrared Spectroscopy. A Bruker IFS 66v/S spectrometer with a spectral resolution of 2 cm^{-1} was used to collect transmission IR spectra of power samples. Approximately 30 mg of solid sample inside a glovebox was pressed into a thin wafer and loaded into a cell that served as a flow reactor (In-situ Research Institute, Inc., South Bend, IN). The cell was sealed and connected to a flow system that allowed recording of spectra while the reactant gases flowed through the cell at reaction temperature. Each spectrum is the average of 64 scans.

2.5. X-ray Absorption Spectroscopy. X-ray absorption spectra were recorded at X-ray beamline 4-1 at the Stanford Synchrotron Radiation Lightsource (SSRL). The storage ring electron energy and ring current were 3 GeV and 300 mA, respectively. A double-crystal Si(220) monochromator was detuned by 20−25% at the Ir L_{III} edge to minimize the effects of higher harmonics in the X-ray beam.

2.6. Catalytic Reaction Rates. Ethylene hydrogenation catalysis was carried out in a conventional laboratory once-through tubular plug-flow reactor at 298 K and 1 bar. The catalyst (10−50 mg) was mixed with 10 g of inert, nonporous α-Al_2O_3 and loaded into the reactor in the argon-filled glovebox. The feed partial pressures were 100 mbar of C_2H_4, 200 mbar of H_2, and 700 mbar of He, with a total flow rate of 100 mL (NTP)/min. Products were analyzed with an online Agilent 6890 gas chromatograph. The ethylene conversions were <5%, and the reactor was well approximated as differential, determining reaction rates directly.

2.7. Computational Methods. Density functional theory (DFT) calculations were performed on neutral cluster models with the M06-L[23] density functional as implemented in the Gaussian 09 software package. In this software package, we used ultrafine grids (99 radial nodes and 590 angular nodes for C, H, and O atoms, but 199 radial nodes and 974 angular nodes for Zr and Ir atoms) for numerical integrations. The def2-svp basis set was used for the C, H, and O atoms, whereas the def2-tzvpp[24−26] basis set and associated effective core potential were employed for Zr and Ir atoms. The positions of all atoms, with the exceptions of the atoms in the aryl organic linkers, were optimized. Vibrational frequency analyses were carried out to confirm the nature of the stationary points found after each geometry optimization. The geometry optimizations and vibrational frequency analyses were carried out for the samples in the gas phase as well as in n-pentane. The polarizable continuum model (PCM^{27}) was used to account for solvation effects for the calculations carried out with the samples in n-pentane.

The cluster models were constructed from periodic unit cells of NU-1000 and UiO-66 optimized with the generalized-gradient approximation PBE[28] density functional while using plane-wave basis sets within the projector-augmented wave approach as implemented in the Vienna Ab Initio Simulation Package (VASP[29−32]). In these periodic calculations, we used a plane-wave kinetic energy cutoff of 520 eV, a convergence criterion of 0.05 eV/Å for atomic positions, and an automatically generated gamma-centered Monkhorst−Pack k-point grid.

The procedure for generating the cluster models from the optimized periodic structure of NU-1000 has been described.[21] Briefly, the first coordination sphere of the Zr_6-metalate node was extracted from the periodic structure while truncating the TPAPy[4−] linkers to benzoate groups. A two-step protocol was then used for optimizing the resulting clusters. First, we optimized the positions of the aromatic H atoms while fixing all other atoms. Second, the C_6H_5 units of the benzoate groups were held fixed, whereas the positions of all other atoms were optimized. A similar procedure was used for UiO-66. However, the linkers in its periodic model were truncated to acetate groups to speed up the computations.

3. RESULTS AND DISCUSSION

3.1. Ir(CO)$_2$ Complexes Supported on Nodes of NU-1000 and of UiO-66.

Ir(CO)$_2$(acac) in n-pentane solution reacted with NU-1000 nodes, removing the protons in hydrogen-bonded H_2O/OH groups,[21] as shown by the decreased intensities of the 2745 cm^{-1} band in the IR spectra (Figure 1B) and forming chemisorbed species assigned on the basis of new IR bands at 2066 and 1990 cm^{-1} as iridium *gem*-dicarbonyls bonded to two ligands inferred to be oxygen atoms also coordinated to the Zr_6 node (Figure 2). The iridium
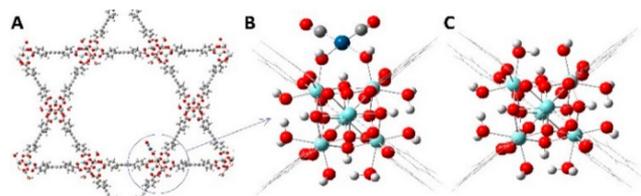
Figure 2. Ir(CO)$_2$ deposited onto the Zr_6 nodes of NU-1000. (A) Location of the iridium complex in a periodic crystal of NU-1000. (B) Expanded view of the iridium complex at the Zr_6 node. (C) Same site in pristine NU-1000 prior to Ir(CO)$_2$ complexation.

loading was 10.0 wt %, corresponding to nearly one Ir atom per node. The ν_{CO} bands shifted to 2017 and 1943 cm^{-1} when the sample was brought in contact with ^{13}CO at room temperature, confirming the identification (Figure S2 and Table S1, Supporting Information). EXAFS parameters measured at the Ir L_{III} edge confirm the structure, with the coordination numbers and interatomic distances shown in Table 1. This structure closely matches that of Ir(CO)$_2$ on a zeolite.[33−36]

Ir(CO)$_2$(acac) in n-pentane solution reacted similarly with UiO-66 nodes, but, in contrast to NU-1000, UiO-66 reacted with Ir(CO)$_2$(acac) to give two chemisorbed species, identified on the basis of IR spectroscopy, with a pair of ν_{CO} bands at 2074 and 1996 cm^{-1}, and a band at 2066 cm^{-1}. Both bands characterizing non-hydrogen-bonded node OH groups, at 3781 and 3692 cm^{-1} (Figure 1A, Table S2), and hydrogen-bonded node H_2O/OH species, at 2745 cm^{-1} (Figure 1B), decreased in intensity as a result of the chemisorption reaction, indicating the participation of these groups, in this case associated with site defects (see below). Correspondingly, the pore volumes of the MOFs decreased (section S4, Supporting Information).

Table 1. EXAFS and Calculated DFT Structural Parameters of Ir(CO)$_2$ Supported on NU-1000 Zr_6 Nodes[a]

shell	$10^3 \times \Delta\sigma^2$ (Å^2)	ΔE_0 (eV)	N	R (Å)	R (Å)
	EXAFS				DFT
Ir−O$_t$	5.4	−5.2	2.0	2.05	2.11
Ir−C$_{CO}$	14.6	−5.9	2.1	1.97	1.83
Ir−O$_{CO}$	14.5	7.4	2.1	2.99	2.98
Ir−O$_b$	6.8	−5.6	1.9	3.13	3.39
Ir−Zr	14.2	−0.7	2.0	3.55	3.72

[a]Notation: O$_t$, O atoms of terminal −OH groups on Zr_6 node; C$_{CO}$, carbonyl carbon; O$_{CO}$, carbonyl oxygen; O$_b$, O in bridging μ_3-OH or μ_3−O group on Zr_6 node; N, coordination number; R, distance between absorber and backscatterer atoms; $\Delta\sigma^2$, disorder term; ΔE_0, inner potential correction. Estimated EXAFS error bounds: N, ±20%; R, ±0.02 Å; $\Delta\sigma^2$, ±20%; ΔE_0, ±20% (Errors characterizing the Ir−Zr contribution are greater.); fit range: 3.87 < k (wave vector) < 13.61 Å^{-1}; 0.5 < R < 4 Å; goodness of fit value = 3.5.

At the high loading of 10 wt % iridium, we also detected physisorbed Ir(CO)$_2$(acac) on each MOF, as shown by the IR bands at 2085 and 2010 cm^{-1} (Figure 1C), which are close in frequency to those characterizing Ir(CO)$_2$(acac) in n-hexane solution.[37] Because the pore aperture of UiO-66 (~6 Å)[18] is barely greater than the narrowest dimension of the precursor (~4 × 6 Å^2), we infer that the supported iridium species were present preferentially near the external UiO-66 particle surfaces.[38,39] The 2010 cm^{-1} band is also evident in the spectrum of the NU-1000-supported species, and it disappeared after 8 h of contact of the precursor with this MOF, during which time two sharp bands at 2082 and 2005 cm^{-1} (also assigned to physisorbed Ir(CO)$_2$(acac) Figure 1C) decreased in intensity and then disappeared after 20 h (Figure S5). Because these disappeared slowly, we suggest that they were indicative of iridium-containing species on the internal NU-1000 surface and that their removal was slowed by their diffusion in the narrow pores.

To determine the structures of the iridium-supporting sites, we performed DFT calculations characterizing the structure of iridium complexes on neutral cluster models of NU-1000. The calculations for NU-1000 show that the most stable iridium complexes are situated in the MOF channels, with the metal atom replacing the proton in a terminal OH$_2$ group that otherwise bridges to an adjacent terminal OH group on the node (Figure 2). This result is consistent with the experimental observation showing a decreased intensity of the H-bonded H_2O and −OH band at 2745 cm^{-1} after reaction of Ir(CO)$_2$(acac) with NU-1000 (Figure 1B). To confirm the assignment of the IR band at 2745 cm^{-1}, we note that DFT predicts that this vibration will be found at approximately 2851 and 2875 cm^{-1}. Application of a scaling factor of 0.956 changes these calculated values to 2726 and 2749 cm^{-1}, in good agreement with the experiment. The choice of this scaling factor is discussed below.

The calculated structural parameters for this binding mode, Figure 2, are compared with EXAFS data in Table 1. Agreement is generally good, although the distances between the Ir atoms and bridging O or Zr atoms of the node are overestimated by 0.2−0.3 Å, consistent with results of analogous combined DFT/EXAFS[40,41] investigations. The calculated ν_{CO} bands of this binding mode are 2157 and 2085 cm^{-1}. Alecu et al.[42] determined scale factors of 0.951−0.958 for fundamental vibrational frequencies obtained with

various M06-L model chemistries; a scaling factor of 0.956 brings the calculated frequencies of the two ν_{CO} bands to 2062 and 1993 cm^{-1}, both within 4 cm^{-1} of experiment, Figure 1C. The calculated separation of the bands (69 cm^{-1} after scaling) matches experiment (76 cm^{-1}) to within 10%.

On UiO-66 (Figure 3A–C), there are three possible types of defects that can be created by the loss of an organic linker
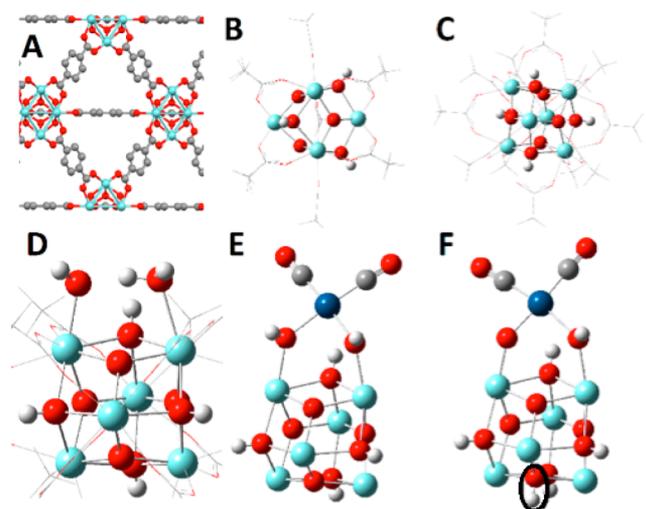
Figure 3. (A) Periodic structure showing the pore channels of UiO-66. (B) Model cluster representing the Zr$_6$ node. (C) Same model cluster rotated 90 deg about the horizontal axis. (D) Ligand defect with terminal −OH and OH$_2$ groups replacing a missing linker. (E) Site 1 complexation of Ir(CO)$_2$. (F) Site 2 complexation of Ir(CO)$_2$ (with "extra" μ_3-OH group circled in black).

(section 8, Supporting Information). The most stable defect is shown in Figure 3D and offers a binding site (site 1) similar to that of NU-1000 (Figure 2C). The decrease of the hydrogen-bonded H$_2$O and −OH band at 2745 cm^{-1} (Figure 1B) indicates the reaction of Ir(CO)$_2$(acac) with site 1 on UiO-66. After bonding of Ir(CO)$_2$ to this defect, Figure 3E, we calculate unscaled ν_{CO} bands of 2165 and 2090 cm^{-1}, very similar to those obtained for NU-1000 and corresponding to the lower-frequency pair observed experimentally, Figure 1C. The structural parameters of this complex are very similar to those in Table 1 for NU-1000. At the M06-L level, formation of Ir(CO)$_2$ supported at site 1 from Ir(CO)$_2$(acac) is calculated to be exoergic by −4.3 kcal/mol.

After consideration of a number of possibilities and an assessment of their energies, we assign the second site (site 2) for adsorption of Ir(CO)$_2$ on UiO-66 as shown in Figure 3F. In this case, a proton has migrated from one coordinating OH group to a μ_3-O oxo group (creating an additional μ_3-OH group, Figure 3F). The above-mentioned non-hydrogen-bonded OH bands at 3781 and 3692 cm^{-1} are calculated to be the hydroxyl groups of site 2 (Table S2). They disappeared after reaction of Ir(CO)$_2$(acac) with these sites. These bands were calculated as being at approximately 3947 and 3875 cm^{-1}, respectively, from our DFT calculations. Again, application of the scaling factor brings good agreement with empirical data (3773 and 3704 cm^{-1}, respectively).

The unscaled calculated ν_{CO} bands for the resulting Ir(CO)$_2$ complex at site 2 are 2173 and 2104 cm^{-1}, corresponding to the higher-frequency pair observed experimentally, Figure 1C. When the scaling factor of 0.956 is applied to the four

computed values (giving 2070 and 1998 cm^{-1} for site 1 and 2077 and 2011 cm^{-1} for site 2), the mean unsigned error compared to experimental values is 8 cm^{-1}, offering good support for these structural assignments. We note that the higher carbonyl stretching frequencies associated with site 2 suggest less back-donation from Ir into acceptor π^*_{CO} orbitals. Consistent with this analysis, calculated partial atomic charges on the Ir center are more positive in site 2 (Hirshfeld:[43] 0.29; Mulliken:[44] 0.51) than in site 1 (Hirshfeld: 0.17; Mulliken: 0.36).

We emphasize that Ir(CO)$_2$(acac) did not react with the bridging μ_3-OH groups on the Zr$_6$ nodes, characterized by the IR band at 3673 cm^{-1}, as indicated by the lack of change of this band, either on NU-1000 or UiO-66, after anchoring of the iridium precursor (Figure 1A). DFT calculations confirm that reaction of Ir(CO)$_2$ groups with the bridging μ_3-OH groups found at defects in UiO-66 is endoergic by about 28 kcal/mol, a value that is in marked contrast to the calculated reaction energies for the adsorption of Ir(CO)$_2$ on site 1 (−4.3 kcal/mol) and site 2 (1.2 kcal/mol).

Ir(CO)$_2$ supported on the MOFs, when treated with flowing C$_2$H$_4$, underwent a limited ligand exchange reaction, sometimes leading to replacement of one CO by C$_2$H$_4$ but only for site 2 in the UiO-66 complex. In that case, a new band at 2020 cm^{-1} was observed and assigned to Ir(CO)(C$_2$H$_4$) (Figure 4).
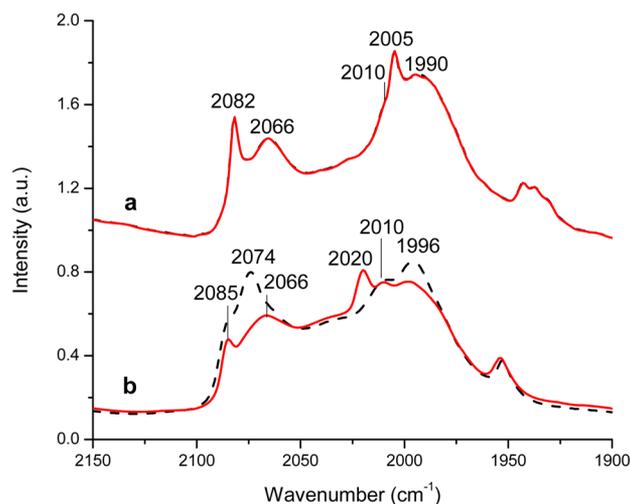
Figure 4. IR spectra in the ν_{CO} region characterizing in the sample initially formed by the chemisorption of Ir(CO)$_2$(acac) on NU-1000 (a) and UiO-66 (b) as initially present (dashed black traces) and after exposure to flowing ethylene at 298 K and 1 bar for 20 min (red traces).

3.2. Ir(C$_2$H$_4$)$_2$ Complexes Supported on the Nodes of NU-1000 and UiO-66.

Supported Ir(C$_2$H$_4$)$_2$ complexes were prepared alternatively from reactions with pristine MOFs employing precursor Ir(C$_2$H$_4$)$_2$(acac) in a fashion analogous to that for Ir(CO)$_2$(acac). IR data (Figures S6 and S7, Supporting Information) indicate that Ir(C$_2$H$_4$)$_2$ also adsorbs onto the nodes, again with single iridium complexes on NU-1000 and a mixture on UiO-66. We sought to prepare supported catalysts dominated by the species analogous to those characterized above, rather than more complex mixtures, by using low loadings of iridium on the supports (1 wt %). At this loading, IR spectra (Figure 5) are consistent with the supports being nearly ideal, and these well-defined samples were tested as
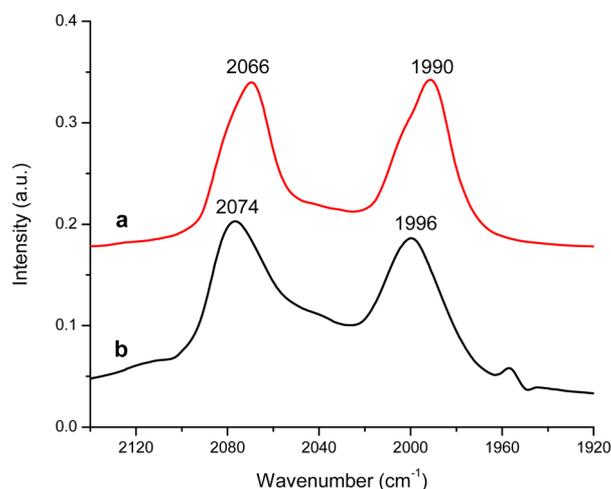
Figure 5. IR spectra in the ν_{CO} region characterizing the sample initially formed by the adsorption of Ir(C2H4)2(acac) (with iridium loading 1%) on NU-1000 (a, red trace) and UiO-66 (b, black trace) after exposure to flowing CO 10%/He at 298 K and 1 bar for 2 min.

catalysts for ethylene conversion in a once-through flow reactor in the presence of H_2 at 300 K and 1 bar.

The supported $Ir(C_2H_4)_2$ complexes were found to be precatalysts for ethylene hydrogenation accompanied by slight ethylene dimerization (Table 2), with the activity and selectivity

Table 2. Catalytic Activities of MOF Node-Supported Iridium Complexes for Hydrogenation and Dimerization of Ethylene in a Flow Reactor at 298 K and 1 bar[a]

		selectivity under differential conversion conditions (mol %)					
					butene isomers		
support[b]	TOF (s^{-1})[c]	ethane	butane	butene	trans-2-butene	1-butene	cis-2-butene
NU-1000	0.010	99.5	0	0.5	0	0.5	0
UiO-66	0.017	98.5	0.4	1.1	0.2	0.8	0.1

[a]There was no detectable reaction in the absence of the catalyst under our conditions, and the MOF alone was catalytically inactive. [b]Support for catalyst initially incorporating node-anchored $Ir(C_2H_4)_2$. [c]Turnover frequency determined from C_2H_4 conversions <5%; catalyst mass = 10−50 mg; feed partial pressures = 100 mbar C_2H_4, 200 mbar H_2, and 700 mbar He; total flow rate = 100 mL (NTP)/min.

both depending on which MOF was used as the support. As noted above, the iridium center of site 2 is more electropositive (or electrophilic) than that of site 1 in the $Ir(CO)_2$ complexes. This pattern extends to the corresponding $Ir(C_2H_4)_2$, $Ir(CO)$-(C_2H_4), $Ir(CO)(C_2H_4)(H_2)$, and $Ir(C_2H_4)_2(H_2)$ species as well. Thus, the nature of the MOF support affects the transition states and activation energies for the various catalytic reactions. In Figure 6, for instance, the calculated barriers for ethylene dimerization catalysis via an intermediate metallacycle are lower for site 2 of UiO-66 than for site 1. Insofar as the NU-1000 catalytic site is analogous to the UiO-66 site 1, Figure 6, this result rationalizes the increased dimerization selectivity observed for UiO-66 and is also consistent with IR data suggesting that site 2 dominates the catalytic reactivity of UiO-66.

Competing reaction mechanisms for ethylene dimerization were explored; the one reported in Figure 6 was found to be energetically the most favorable. The pathway for ethylene
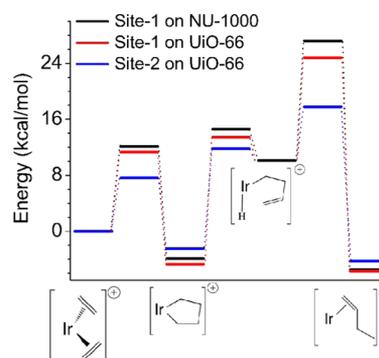
Figure 6. Calculated pathway for the dimerization of ethylene to 1-butene at sites 1 and 2 for $Ir(C_2H_4)_2$ on UiO-66 and NU-1000 at M06-L level. (MOF nodes as counteranions are implicit.) More details are available in section S8 of the Supporting Information.

hydrogenation was also investigated, and the results show that hydrogenation is favored over dimerization because of the lower calculated barriers (2−12 kcal/mol for hydrogenation, section S8, Supporting Information, versus 8−19 kcal/mol for dimerization, Figure 6) and the weak adsorption of ethane on the iridium sites (relative to alkenes), which favors desorption of this product, Table 2.

We probed the used catalysts (after 1 h of continuous ethylene hydrogenation) with a pulse of CO introduced into the feed stream. The results (Figure S8, Supporting Information) indicate the formation of the iridium *gem*-dicarbonyl bands essentially matching those of the fresh catalyst, thereby demonstrating the stability of the mononuclear iridium complexes under catalytic reaction conditions.

4. CONCLUSIONS

The nodes of NU-1000 and UiO-66 MOFs are essentially molecular catalyst supports upon which highly uniform catalytic metal complexes can be chemisorbed. These are among the simplest and best-defined of any supported metal species, constituting, we infer, an emerging class of materials that may offer broad opportunities for discovery of new catalysts guided by theory. We may expect high selectivities associated with the uniformity of the catalytic species and high stabilities when combinations of metals and MOFs are appropriately chosen.

■ ASSOCIATED CONTENT

Ⓢ Supporting Information

Experimental and computational details as reported in the text. The Supporting Information is available free of charge on the ACS Publications website at DOI: 10.1021/jacs.5b02956.

■ AUTHOR INFORMATION

Corresponding Authors

*gagliard@umn.edu
*bcgates@ucdavis.edu

Notes

The authors declare no competing financial interest.

■ ACKNOWLEDGMENTS

■ REFERENCES

(1) Furukawa, H.; Cordova, K. E.; O'Keeffe, M.; Yaghi, O. M. *Science* **2013**, *341*, 974.

(2) Ferey, G. *Chem. Soc. Rev.* **2008**, *37*, 191.

(3) Horike, S.; Shimomura, S.; Kitagawa, S. *Nat. Chem.* **2009**, *1*, 695.

(4) Corma, A.; Garcia, H.; Llabres i Xamena, F. X. *Chem. Rev.* **2010**, *110*, 4606.

(5) Lee, J.; Farha, O. K.; Roberts, J.; Scheidt, K. A.; Nguyen, S. T.; Hupp, J. T. *Chem. Soc. Rev.* **2009**, *38*, 1450.

(6) Gascon, J.; Corma, A.; Kapteijn, F.; Llabres i Xamena, F. X. *ACS Catal.* **2014**, *4*, 361.

(7) Farrusseng, D.; Aguado, S.; Pinel, C. *Angew. Chem., Int. Ed.* **2009**, *48*, 7502.

(8) Dhakshinamoorthy, A.; Alvaro, M.; Garcia, H. *Catal. Sci. Technol.* **2011**, *1*, 856.

(9) Ma, L. Q.; Abney, C.; Lin, W. B. *Chem. Soc. Rev.* **2009**, *38*, 1248.

(10) Yoon, M.; Srirambalaji, R.; Kim, K. *Chem. Rev.* **2012**, *112*, 1196.

(11) Manna, K.; Zhang, T.; Carboni, M.; Abney, C. W.; Lin, W. B. *J. Am. Chem. Soc.* **2014**, *136*, 13182.

(12) Fei, H. H.; Cohen, S. M. *J. Am. Chem. Soc.* **2015**, *137*, 2191.

(13) Gonzalez, M. I.; Bloch, E. D.; Mason, J. A.; Teat, S. J.; Long, J. R. *Inorg. Chem.* **2015**, *54*, 2995.

(14) Larabi, C.; Quadrelli, E. A. *Eur. J. Inorg. Chem.* **2012**, 3014.

(15) Nguyen, H. G. T.; Schweitzer, N. M.; Chang, C. Y.; Drake, T. L.; So, M. C.; Stair, P. C.; Farha, O. K.; Hupp, J. T.; Nguyen, S. T. *ACS Catal.* **2014**, *4*, 2496.

(16) Mondloch, J. E.; Bury, W.; Fairen-Jimenez, D.; Kwon, S.; DeMarco, E. J.; Weston, M. H.; Sarjeant, A. A.; Nguyen, S. T.; Stair, P. C.; Snurr, R. Q.; Farha, O. K.; Hupp, J. T. *J. Am. Chem. Soc.* **2013**, *135*, 10294.

(17) Serna, P.; Gates, B. C. *Acc. Chem. Res.* **2014**, *47*, 2612.

(18) Cavka, J. H.; Jakobsen, S.; Olsbye, U.; Guillou, N.; Lamberti, C.; Bordiga, S.; Lillerud, K. P. *J. Am. Chem. Soc.* **2008**, *130*, 13850.

(19) Cliffe, M. J.; Wan, W.; Zou, X. D.; Chater, P. A.; Kleppe, A. K.; Tucker, M. G.; Wilhelm, H.; Funnell, N. P.; Coudert, F.-X.; Goodwin, A. L. *Nat. Commun.* **2014**, *5*, 4176.

(20) Vermoortele, F.; Bueken, B.; Le Bars, G.; Van de Voorde, B.; Vandichel, M.; Houthoofd, K.; Vimont, A.; Daturi, M.; Waroquier, M.; Van Speybroeck, V.; Kirschhock, C.; De Vos, D. E. *J. Am. Chem. Soc.* **2013**, *135*, 11465.

(21) Planas, N.; Mondloch, J. E.; Tussupbayev, S.; Borycz, J.; Gagliardi, L.; Hupp, J. T.; Farha, O. K.; Cramer, C. J. *J. Phys. Chem. Lett.* **2014**, *5*, 3716.

(22) Bhirud, V. A.; Uzun, A.; Kletnieks, P. W.; Craciun, R.; Haw, J. F.; Dixon, D. A.; Olmstead, M. M.; Gates, B. C. *J. Organomet. Chem.* **2007**, *692*, 2107.

(23) Zhao, Y.; Truhlar, D. G. *J. Chem. Phys.* **2006**, *125*, 194101.

(24) Metz, B.; Stoll, H.; Dolg, M. *J. Chem. Phys.* **2000**, *113*, 2563.

(25) Weigend, F. *Phys. Chem. Chem. Phys.* **2006**, *8*, 1057.

(26) Weigend, F.; Ahlrichs, R. *Phys. Chem. Chem. Phys.* **2005**, *7*, 3297.

(27) Cossi, M.; Rega, N.; Scalmani, G.; Barone, V. *J. Comput. Chem.* **2003**, *24*, 669.

(28) Perdew, J. P.; Burke, K.; Ernzerhof, M. *Phys. Rev. Lett.* **1996**, *77*, 3865.

(29) Kresse, G.; Furthmuller, J. *Phys. Rev. B* **1996**, *54*, 11169.

(30) Kresse, G.; Hafner, J. *Phys. Rev. B* **1994**, *49*, 14251.

(31) Kresse, G.; Hafner, J. *Phys. Rev. B* **1993**, *47*, 558.

(32) Kresse, G.; Furthmuller, J. *Comp. Mater. Sci.* **1996**, *6*, 15.

(33) Lu, J.; Serna, P.; Aydin, C.; Browning, N. D.; Gates, B. C. *J. Am. Chem. Soc.* **2011**, *133*, 16186.

(34) Miessner, H. *J. Am. Chem. Soc.* **1994**, *116*, 11522.

(35) Uzun, A.; Bhirud, V. A.; Kletnieks, P. W.; Haw, J. F.; Gates, B. C. *J. Phys. Chem. C* **2007**, *111*, 15064.

(36) Wu, H.; Chua, Y. S.; Krungleviciute, V.; Tyagi, M.; Chen, P.; Yildirim, T.; Zhou, W. *J. Am. Chem. Soc.* **2013**, *135*, 10525.

(37) Bonati, F.; Ugo, R. *J. Organomet. Chem.* **1968**, *11*, 341.

(38) Lu, J.; Aydin, C.; Browning, N. D.; Gates, B. C. *Langmuir* **2012**, *28*, 12806.

(39) Ogino, I.; Chen, C. Y.; Gates, B. C. *Dalton Trans.* **2010**, *39*, 8423.

(40) Delgado, M.; Santini, C. C.; Delbecq, F.; Baudouin, A.; De Mallmann, A.; Prestipino, C.; Norsic, S.; Sautet, P.; Basset, J.-M. *J. Phys. Chem. C* **2011**, *115*, 6757.

(41) Williams, L. A.; Guo, N.; Motta, A.; Delferro, M.; Fragala, I. L.; Miller, J. T.; Marks, T. J. *Proc. Natl. Acad. Sci. U.S.A.* **2013**, *110*, 413.

(42) Alecu, I. M.; Zheng, J. J.; Zhao, Y.; Truhlar, D. G. *J. Chem. Theory Comput.* **2010**, *6*, 2872.

(43) Hirshfeld, F. L. *Theor. Chem. Acc.* **1977**, *44*, 129.

(44) Mulliken, R. S. *J. Chem. Phys.* **1955**, *23*, 1833.